PROCEEDINGS A

royalsocietypublishing.org/journal/rspa

Research

Cite this article: Su Y, Chen W, Dorfmann L, Destrade M. 2020 The effect of an exterior electric field on the instability of dielectric plates. *Proc. R. Soc. A* **476**: 20200267. http://dx.doi.org/10.1098/rspa.2020.0267

Received: 11 April 2020
Accepted: 5 June 2020

Subject Areas:
applied mathematics, electromagnetism, mechanics

Keywords:
nonlinear electro-elasticity, electro-elastic plate instability, exterior electric field, Stroh method

Author for correspondence:
Yipin Su
e-mail: su_yp@zju.edu.cn

Electronic supplementary material is available online at https://doi.org/10.6084/m9.figshare.c.5056721.

THE ROYAL SOCIETY PUBLISHING

The effect of an exterior electric field on the instability of dielectric plates

Yipin Su[1,2], Weiqiu Chen[1], Luis Dorfmann[3] and Michel Destrade[1,2]

[1]Department of Engineering Mechanics, Zhejiang University, Hangzhou 310027, People's Republic of China
[2]Stokes Centre for Applied Mathematics, School of Mathematics, Statistics and Applied Mathematics, NUI Galway, University Road, Galway, Ireland
[3]Department of Civil and Environmental Engineering, Tufts University, Medford, MA 02155, USA

YS, 0000-0002-5583-4251; MD, 0000-0002-6266-1221

We investigate the theoretical nonlinear response, Hessian stability, and possible wrinkling behaviour of a voltage-activated dielectric plate immersed in a tank filled with silicone oil. Fixed rigid electrodes are placed on the top and bottom of the tank, and an electric field is generated by a potential difference between the electrodes. We solve the associated incremental boundary value problem of superimposed, inhomogeneous small-amplitude wrinkles, signalling the onset of instability. We decouple the resulting bifurcation equation into symmetric and antisymmetric modes. For a neo-Hookean dielectric plate, we show that a potential difference between the electrodes can induce a thinning of the plate and thus an increase of its planar area, similar to the scenarios encountered when there is no silicone oil. However, we also find that, depending on the material and geometric parameters, an increasing applied voltage can also lead to a *thickening* of the plate, and thus a shrinking of its area. In that scenario, Hessian instability and wrinkling bifurcation may then occur spontaneously once some critical voltages are reached.

1. Introduction

Dielectric elastomers (DEs) are soft materials capable of undergoing large deformations when activated by an

electric field. Compared with other 'smart' materials such as, for example, electro-active ceramics and shape memory alloys, DEs have the advantages of high sensitivity, low noise and large actuation strains. They have potential applications as sensors, as artificial muscles and as biologically inspired intelligent devices [1–3].

Typically, a planar dielectric actuator consists of a thin electro-elastic plate with two electrodes coated on its main surfaces. Carbon grease or a conductive hydrogel are frequently used as electrodes. These coated films are thin and highly flexible and do not constrain the deformation of the actuator, hence play no noticeable mechanical role. Applying a potential difference [4–6] or a surface charge density [7,8] on the electrodes generates electrostatic forces causing a reduction in thickness and therefore, by incompressibility, a planar expansion. When the thickness of the plate is small compared to the planar dimensions, there is no electric field outside the plate by Gauss's theorem.

Another possible actuation is obtained by immersing a dielectric plate in a conductive fluid, with the electric field generated by a potential difference or by a surface charge density on two rigid electrodes positioned appropriately. Notable applications of that set-up include biometric sensors and wearable or implantable electronic devices. For example, Sun *et al.* [9] designed an 'ionic skin' consisting of a stretchable dielectric membrane sandwiched between two flexible ionic conductors using rigid electrodes. Their device operates as a strain sensor and can be used to detect the location and pressure of human touch. Liquid crystal elastomers and ionic electro-active polymers are considered electro-active elastomers with potential applications in display technologies and drug delivery systems [10]. Bioelectrical and mechanical interactions exist in biological tissues such as bones, vessels and nerve cells [11,12] and, more recently, have been identified as powerful tools of biological pattern control [13]. For an electro-active elastomer immersed in a conductive medium with non-zero permittivity, the surrounding electric field has an obvious and significant influence on the mechanical response of the plate.

Advanced theories to describe the main electro-mechanical phenomena observed in DEs have been developed over the years, including nonlinear deformation [14,15], vibration [16–18], wrinkling instability [19–21] and wave propagation [22–24]. Most of these studies focused on electro-elastic plates actuated by flexible electrodes. In contrast, little attention has been devoted to devices actuated by an external electric field.

Dorfmann & Ogden [25] studied the large plane strain deformation and instability of an electro-elastic half-space in the presence of a uniform external electric field normal to its surface. Subsequently, they studied the instability of an equi-biaxially deformed dielectric plate, without flexible electrodes, but in the presence of an external electric field normal to its faces [26]. Chen & Dai [27] investigated the propagation of axisymmetric waves in a homogeneously deformed dielectric cylinder subject to an external electric field oriented along the axial direction and derived the exact wave solution in terms of Bessel functions. Su *et al.* [28,29] examined the propagation of non-axisymmetric waves in, and the instability of, an electro-active hollow cylinder under uniform mechanical and electrical fields. They found that the exterior electric field can have a stabilizing or destabilizing influence, depending on the electro-elastic coupling parameters of the materials. Note that in these studies the DEs were surrounded by vacuum to simplify the forms of the governing equations and of the boundary conditions.

Díaz-Calleja *et al.* [30] compared the pull-in instabilities of an electro-elastic plate with two flexible electrodes coated on its faces and of a dielectric plate floating between two fixed rigid electrodes. They investigated the effect of the permittivity of the surrounding fluid on the stability of the elastomer. They focused on homogeneous instabilities only and did not include inhomogeneous wrinkling-type modes. Wang *et al.* [31] observed experimentally that instabilities occur in a substrate-bonded elastomer film immersed in a conductive solution sandwiched between electrodes when the applied voltage exceeds a critical value. They predicted the critical field for instability by comparing the potential energies in the wrinkled and flat states. However, they did not consider the mechanical role of the conductive solution.

Su *et al.* [21] studied the nonlinear deformation and wrinkling behaviour of a dielectric plate sandwiched between two compliant electrodes (figure 1*a*). They found that a superposed

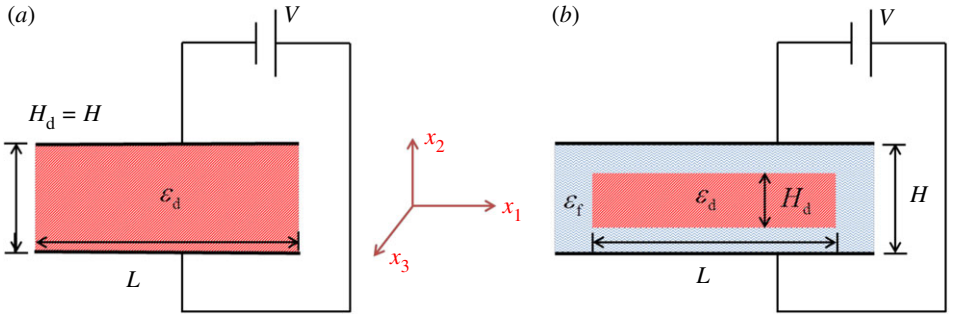

Figure 1. Loading scenarios for an electro-elastic plate. In (*a*) the electric field is generated by a potential difference between two flexible electrodes coated on the main faces; in (*b*) the plate is immersed in a tank filled with silicone oil with the electric field generated by two rigid electrodes placed at the top and bottom of the tank. (Online version in colour.)

mechanical load is required to induce wrinkling of the plate. In this paper, we consider a DE plate immersed in silicone oil (figure 1*b*). In particular, we show that the plate can lose stability by applying a voltage only, due to electrostriction.

Consider a rectangular electro-elastic plate with permittivity ε_d and with reference thickness H_d. Following the application of an electric field, the resulting deformation is homogeneous and defined in terms of the principal stretches λ_1, λ_2, λ_3. The material is incompressible, so that the change in thickness is defined by the stretch $\lambda_2 = \lambda_1^{-1}\lambda_3^{-1}$. Hence, the deformed plate has uniform thickness

$$h_d = \lambda_2 H_d = \lambda_1^{-1}\lambda_3^{-1} H_d. \tag{1.1}$$

For a DE plate immersed in a tank filled with silicone oil having an electric permittivity ε_f, the electric field is generated by a potential difference, say V, between two fixed rigid electrodes placed on the top and bottom of the tank. The distance between the two electrodes is constant and denoted H. It follows that

$$E_0 H_d + E^\star (H - h_d) = V, \tag{1.2}$$

where E_0 is the nominal electric field in the plate and $E^\star$ denotes the electric field in the silicone oil. Throughout the paper we use the star superscript * to denote quantities defined in the oil, outside the region occupied by the plate.

The paper is organized as follows. In §2 we present the equations governing the equilibrium of an electro-elastic plate and specialize the boundary conditions to the set-up considered here (figure 1*b*).

Then, in §3, we extend the method of Su *et al.* [21] to include the effect of an exterior electric field. Hence we consider a two-dimensional incremental displacement superposed upon the large equi-biaxial deformation. Specifically, we look for small sinusoidal variations in the x_1-direction with exponential variation in the x_2-direction and rewrite the incremental equations in the Stroh form to solve the corresponding boundary value problem. We manage to factorize the resulting wrinkling equation of the plate into symmetric and antisymmetric modes.

In §4 we consider the equilibrium of an equi-biaxially deformed electro-elastic plate and its stability, when the material is modelled by the neo-Hookean dielectric model. We derive explicitly the bifurcation criterion for neo-Hookean electro-elastic plates of finite thickness and its specializations in the thin-plate and thick-plate limits. Our numerical results elucidate the influences of the material properties of the silicone oil and of the elastomer on the nonlinear response and on the instability behaviour of the electro-elastic plate. In particular we find scenarios where the immersed plate (figure 1*b*) can be made to wrinkle by voltage alone, a possibility that does not arise when there is no exterior field (figure 1*a*). We give concluding remarks in §5.

2. Large actuation

According to the nonlinear theory of electro-elasticity [32–34], for an incompressible dielectric plate in mechanical and electrostatic equilibrium, we find that

$$\tau_{11}-\tau_{22}=\lambda_1\frac{\partial W}{\partial \lambda_1},\quad \tau_{33}-\tau_{22}=\lambda_3\frac{\partial W}{\partial \lambda_3},\quad D_0=-\frac{\partial W}{\partial E_0}, \tag{2.1}$$

where τ_{ii} $(i=1,2,3)$ is the principal component of the total Cauchy stress tensor of the solid in the x_i-direction, $W(\lambda_1,\lambda_3,E_0)$ is the energy density of the elastomer and D_0 is the non-zero component of the nominal electric displacement field in the x_2-direction inside the plate.

The true electric displacement D in the plate is connected to its nominal counterpart D_0 by

$$D=\lambda_1^{-1}\lambda_3^{-1}D_0=-\lambda_1^{-1}\lambda_3^{-1}\frac{\partial W}{\partial E_0}. \tag{2.2}$$

The normal component of the electric displacement, in the absence of free surface charge, is continuous across a material interface. It follows that

$$D^\star=D=-\lambda_1^{-1}\lambda_3^{-1}\frac{\partial W}{\partial E_0}, \tag{2.3}$$

where $D^\star$ denotes the electric displacement in the silicone oil in the x_2-direction. The electric field in the silicone oil can now be determined as

$$E^\star=\varepsilon_{\mathrm{f}}^{-1}D^\star=-\varepsilon_{\mathrm{f}}^{-1}\lambda_1^{-1}\lambda_3^{-1}\frac{\partial W}{\partial E_0}, \tag{2.4}$$

so that equation (1.2) reads

$$E_0H_{\mathrm{d}}-\varepsilon_{\mathrm{f}}^{-1}\lambda_1^{-1}\lambda_3^{-1}\frac{\partial W}{\partial E_0}(H-\lambda_1^{-1}\lambda_3^{-1}H_{\mathrm{d}})=V. \tag{2.5}$$

For a given energy function $W(\lambda_1,\lambda_3,E_0)$, the nominal electric field in the plate E_0 is then obtained from equation (2.5).

The non-zero components of the Maxwell stress tensor in the silicone oil have the forms [26]

$$\tau_{11}^\star=\tau_{33}^\star=-\tau_{22}^\star=-\frac{1}{2\varepsilon_{\mathrm{f}}}\left(D^\star\right)^2=-\frac{1}{2\varepsilon_{\mathrm{f}}}\lambda_1^{-2}\lambda_3^{-2}\left(\frac{\partial W}{\partial E_0}\right)^2. \tag{2.6}$$

Assume that the plate is subject to in-plane biaxial nominal stresses s_1 and s_3 in the x_1- and x_3-directions, respectively, with its main surfaces $x_2=\pm h_{\mathrm{d}}/2$ being traction-free. The mechanical continuity condition gives

$$s_1=\lambda_1^{-1}\left(\tau_{11}-\tau_{11}^\star\right),\quad s_3=\lambda_3^{-1}\left(\tau_{33}-\tau_{33}^\star\right),\quad \tau_{22}=\tau_{22}^\star. \tag{2.7}$$

Finally, combining equations (2.1) and (2.7) yields the equations governing the nonlinear response of the electro-elastic plate:

$$\frac{\partial W}{\partial \lambda_1}+\lambda_1^{-1}\left(\tau_{22}^\star-\tau_{11}^\star\right)=s_1,\quad \frac{\partial W}{\partial \lambda_3}+\lambda_3^{-1}\left(\tau_{22}^\star-\tau_{33}^\star\right)=s_3. \tag{2.8}$$

3. Linearized stability analysis

(a) Stroh formulation

In this section we use the linearized incremental theory of electro-elasticity to predict the onset of wrinkling instability for the actuated electro-elastic plate [25,29,35–38]. Here and in the following, we use a superimposed dot to denote increments.

Superimpose a small-amplitude mechanical perturbation $\mathbf{u}=\dot{\mathbf{x}}$ along with an updated incremental electric field $\dot{\mathbf{E}}$ upon the finitely deformed configuration. The corresponding updated incremental electric displacement field is $\dot{\mathbf{D}}$. We look for incremental two-dimensional solutions independent of x_3. A simple analysis then shows that $u_3=\dot{E}_3=\dot{D}_3=0$.

The incremental electric field is irrotational and, therefore, it can be expressed as

$$\dot{E}_1 = -\frac{\partial \dot{\phi}}{\partial x_1}, \qquad \dot{E}_2 = -\frac{\partial \dot{\phi}}{\partial x_2}, \tag{3.1}$$

where $\dot{\phi}$ is the incremental electric potential in the plate.

Following Su *et al.* [21], we seek solutions of the incremental equilibrium equations that vary sinusoidally along the x_1-direction with amplitude variations in the x_2-direction. We use the form

$$\{u_1, u_2, \dot{D}_2, \dot{T}_{21}, \dot{T}_{22}, \dot{\phi}\} = \Re\left\{\left[k^{-1}U_1, k^{-1}U_2, \mathrm{i}\Delta, \mathrm{i}\Sigma_{21}, \mathrm{i}\Sigma_{22}, k^{-1}\Phi\right] e^{\mathrm{i}kx_1}\right\}, \tag{3.2}$$

where $\dot{T}_{21}$, $\dot{T}_{22}$ are the components of the updated incremental nominal stress, U_1, U_2, Δ, Σ_{21}, Σ_{22}, Φ are functions of kx_2 only, and $k = 2\pi/\mathcal{L}$ is the wavenumber with $\mathcal{L}$ being the wavelength of the wrinkles of the buckled plate.

It is convenient to rewrite the boundary value problem in the Stroh form:

$$\boldsymbol{\eta}' = \mathrm{i}\mathbf{N}\boldsymbol{\eta} = \mathrm{i}\begin{bmatrix} \mathbf{N}_1 & \mathbf{N}_2 \\ \mathbf{N}_3 & \mathbf{N}_1^T \end{bmatrix}\boldsymbol{\eta}, \tag{3.3}$$

where $\mathrm{i}^2 = -1$, $\mathbf{N}$ is the Stroh matrix, $\boldsymbol{\eta} = [U_1 \;\; U_2 \;\; \Delta \;\; \Sigma_{21} \;\; \Sigma_{22} \;\; \Phi]^T$ is the Stroh vector [21,39], and the prime denotes differentiation with respect to kx_2. In what follows we use the notation $\boldsymbol{\eta} = [\mathbf{U}\ \mathbf{S}]^T$, where $\mathbf{U} = [U_1 \; U_2 \; \Delta]^T$ and $\mathbf{S} = [\Sigma_{21} \; \Sigma_{22} \; \Phi]^T$ represent the generalized displacement and traction vectors, respectively. Here we find that the 3×3 sub-blocks $\mathbf{N}_1$, $\mathbf{N}_2$ and $\mathbf{N}_3$ have the components

$$\left.\begin{aligned} \mathbf{N}_1 &= \begin{bmatrix} 0 & -1+\tau_{22}/c & 0 \\ -1 & 0 & 0 \\ 0 & \mathrm{d}\tau_{22}/c & 0 \end{bmatrix}, \quad \mathbf{N}_2 = \begin{bmatrix} 1/c & 0 & d/c \\ 0 & 0 & 0 \\ d/c & 0 & d^2/c - f \end{bmatrix} \\ \text{and} \qquad \mathbf{N}_3 &= \begin{bmatrix} -2(b+c-\tau_{22}) + e^2/g & 0 & -e/g \\ 0 & -a + (c-\tau_{22})^2/c & 0 \\ -e/g & 0 & 1/g \end{bmatrix}, \end{aligned}\right\} \tag{3.4}$$

where a, b, c, d, e, f, g are electro-elastic coefficients evaluated for a prescribed finite deformation and for a given material model; see [21] for their general expressions.

Because the Stroh matrix $\mathbf{N}$ is constant, the solution to equation (3.3) is of the exponential form,

$$\boldsymbol{\eta}(kx_2) = \begin{bmatrix} \mathbf{U}(kx_2) \\ \mathbf{S}(kx_2) \end{bmatrix} = \sum_{j=1}^{6} c_j \boldsymbol{\eta}^{(j)} e^{\mathrm{i}q_j kx_2}, \tag{3.5}$$

where c_j, $j = 1, 2, \ldots, 6$, are arbitrary constants to be determined and q_j, $j = 1, \ldots, 6$, are the eigenvalues found by solving the characteristic equation

$$\det(\mathbf{N} - q\mathbf{I}) = 0. \tag{3.6}$$

The eigenvectors $\boldsymbol{\eta}^{(j)}$, $j = 1, 2, \ldots, 6$, associated with q_j are connected through the relation $\boldsymbol{\eta}^{(j)} = (\boldsymbol{\eta}^{(j+3)})^*$, $j = 1, 2, 3$, where the asterisk denotes the complex conjugate. Note that for the model used in the next section (neo-Hookean model) we have the connections $q_j = \mathrm{i}p_j$ and $q_{j+3} = -\mathrm{i}p_j$, $j = 1, 2, 3$ with real p_j.

We now write the generalized displacement and traction vectors at the faces $x_2 = \pm h_\mathrm{d}/2$ in the forms

$$\begin{bmatrix} \mathbf{U}(kh_\mathrm{d}/2) \\ \mathbf{U}(-kh_\mathrm{d}/2) \end{bmatrix} = \begin{bmatrix} \eta_1^{(1)}E_1^- & \eta_1^{(2)}E_2^- & \eta_1^{(3)}E_3^- & \eta_1^{(4)}E_1^+ & \eta_1^{(5)}E_2^+ & \eta_1^{(6)}E_3^+ \\ \eta_2^{(1)}E_1^- & \eta_2^{(2)}E_2^- & \eta_2^{(3)}E_3^- & \eta_2^{(4)}E_1^+ & \eta_2^{(5)}E_2^+ & \eta_2^{(6)}E_3^+ \\ \eta_3^{(1)}E_1^- & \eta_3^{(2)}E_2^- & \eta_3^{(3)}E_3^- & \eta_3^{(4)}E_1^+ & \eta_3^{(5)}E_2^+ & \eta_3^{(6)}E_3^+ \\ \eta_1^{(1)}E_1^+ & \eta_1^{(2)}E_2^+ & \eta_1^{(3)}E_3^+ & \eta_1^{(4)}E_1^- & \eta_1^{(5)}E_2^- & \eta_1^{(6)}E_3^- \\ \eta_2^{(1)}E_1^+ & \eta_2^{(2)}E_2^+ & \eta_2^{(3)}E_3^+ & \eta_2^{(4)}E_1^- & \eta_2^{(5)}E_2^- & \eta_2^{(6)}E_3^- \\ \eta_3^{(1)}E_1^+ & \eta_3^{(2)}E_2^+ & \eta_3^{(3)}E_3^+ & \eta_3^{(4)}E_1^- & \eta_3^{(5)}E_2^- & \eta_3^{(6)}E_3^- \end{bmatrix} \begin{bmatrix} c_1 \\ c_2 \\ c_3 \\ c_4 \\ c_5 \\ c_6 \end{bmatrix} \tag{3.7}$$

and

$$\begin{bmatrix} \mathbf{S}(kh_\mathrm{d}/2) \\ \mathbf{S}(-kh_\mathrm{d}/2) \end{bmatrix} = \begin{bmatrix} \eta_4^{(1)}E_1^- & \eta_4^{(2)}E_2^- & \eta_4^{(3)}E_3^- & \eta_4^{(4)}E_1^+ & \eta_4^{(5)}E_2^+ & \eta_4^{(6)}E_3^+ \\ \eta_5^{(1)}E_1^- & \eta_5^{(2)}E_2^- & \eta_5^{(3)}E_3^- & \eta_5^{(4)}E_1^+ & \eta_5^{(5)}E_2^+ & \eta_5^{(6)}E_3^+ \\ \eta_6^{(1)}E_1^- & \eta_5^{(2)}E_2^- & \eta_5^{(3)}E_3^- & \eta_5^{(4)}E_1^+ & \eta_5^{(5)}E_2^+ & \eta_5^{(6)}E_3^+ \\ \eta_4^{(1)}E_1^+ & \eta_4^{(2)}E_2^+ & \eta_4^{(3)}E_3^+ & \eta_4^{(4)}E_1^- & \eta_4^{(5)}E_2^- & \eta_4^{(6)}E_3^- \\ \eta_5^{(1)}E_1^+ & \eta_5^{(2)}E_2^+ & \eta_5^{(3)}E_3^+ & \eta_5^{(4)}E_1^- & \eta_5^{(5)}E_2^- & \eta_5^{(6)}E_3^- \\ \eta_6^{(1)}E_1^+ & \eta_6^{(2)}E_2^+ & \eta_6^{(3)}E_3^+ & \eta_6^{(4)}E_1^- & \eta_6^{(5)}E_2^- & \eta_6^{(6)}E_3^- \end{bmatrix} \begin{bmatrix} c_1 \\ c_2 \\ c_3 \\ c_4 \\ c_5 \\ c_6 \end{bmatrix}, \tag{3.8}$$

where $\eta_i^{(j)}$, $i,j = 1,2,\ldots,6$ is the ith component of the eigenvector $\boldsymbol{\eta}^{(j)}$, $E_j^\pm = e^{\pm p_j k h_\mathrm{d}/2}$, for $j = 1,\ldots,6$, and the relation $E_{j+3}^\pm = E_j^\mp$, $j = 1,2,3$ holds. Su *et al.* [21] showed that for the neo-Hookean, Mooney–Rivlin and Gent energy functions, the following relationships apply:

$$\begin{aligned} &\eta_1^{(j)} = -\eta_1^{(j+3)}, \quad \eta_2^{(j)} = \eta_2^{(j+3)}, \quad \eta_3^{(j)} = -\eta_3^{(j+3)}, \\ &\eta_4^{(j)} = \eta_4^{(j+3)}, \quad \eta_5^{(j)} = -\eta_5^{(j+3)}, \quad \eta_6^{(j)} = \eta_6^{(j+3)}. \end{aligned} \tag{3.9}$$

(b) Bifurcation equation for wrinkles

The total Cauchy stress tensor used in the Stroh matrix (3.4) has the form

$$\tau_{22} = \tau_{22}^\star = \frac{1}{2\varepsilon_\mathrm{f}} D^2, \tag{3.10}$$

with the incremental interfacial conditions at $x_2 = \pm h_\mathrm{d}/2$ given by

$$\begin{aligned} &\dot{T}_{21} = -\tau_{11}^\star u_{2,1} + \dot{\tau}_{21}^\star, \quad \dot{T}_{22} = -\tau_{22}^\star u_{2,2} + \dot{\tau}_{22}^\star, \\ &\dot{D}_2 = \dot{D}_2^\star - D^\star u_{2,2}, \qquad \dot{E}_1 = \dot{E}_1^\star + E_2^\star u_{2,1}. \end{aligned} \tag{3.11}$$

It is convenient to introduce the incremental electric potential in the silicone oil, denoted $\dot{\phi}^\star$. The non-zero components of the incremental external electric field and the corresponding incremental electric displacements are then calculated as

$$\dot{E}_1^\star = -\frac{\partial \dot{\phi}^\star}{\partial x_1}, \quad \dot{E}_2^\star = -\frac{\partial \dot{\phi}^\star}{\partial x_2} \tag{3.12}$$

and

$$\dot{D}_1^\star = -\varepsilon_\mathrm{f} \frac{\partial \dot{\phi}^\star}{\partial x_1}, \quad \dot{D}_2^\star = -\varepsilon_\mathrm{f} \frac{\partial \dot{\phi}^\star}{\partial x_2}, \tag{3.13}$$

respectively.

Since the applied voltage is fixed, the boundary conditions on the top and bottom faces of the tank read

$$\dot{\phi}^{\star}(x_1, \pm H/2) = 0. \tag{3.14}$$

The incremental form of Maxwell's equation outside the material simplifies to $\mathrm{div}\dot{\mathbf{D}}^{\star} = 0$ and the incremental electric potential $\dot{\phi}^{\star}$ thus satisfies the Laplace equation

$$\frac{\partial^2 \dot{\phi}^{\star}}{\partial x_1^2} + \frac{\partial^2 \phi^{\star}}{\partial x_2^2} = 0. \tag{3.15}$$

It follows that the incremental electric potential for the silicone oil in the region $H/2 \le x_2 \le h_{\mathrm{d}}/2$ is of the form

$$\dot{\phi}_{+}^{\star}(x_1, x_2) = k^{-1}\left(C_1^{\star} e^{kx_2} + C_2^{\star} e^{-kx_2}\right) e^{\mathrm{i}kx_1}, \tag{3.16}$$

where $C_1^{\star}$ and $C_2^{\star}$ are constants of integration, to be determined from the incremental interfacial and boundary conditions.

Following Dorfmann & Ogden [26], we write the non-zero components of the associated incremental Maxwell stress tensor as

$$\dot{\tau}_{11}^{\star} = \dot{\tau}_{33}^{\star} = -\dot{\tau}_{22}^{\star} = D\frac{\partial \dot{\phi}_{+}^{\star}}{\partial x_2}, \qquad \dot{\tau}_{12}^{\star} = \dot{\tau}_{21}^{\star} = -D\frac{\partial \dot{\phi}_{+}^{\star}}{\partial x_1}. \tag{3.17}$$

Substitution of equations (2.3), (3.2), (3.13) and (3.16) into the interfacial conditions equation $(3.11)_3$ gives the connection

$$C_1^{\star} e^{kh_{\mathrm{d}}/2} - C_2^{\star} e^{-kh_{\mathrm{d}}/2} = \mathrm{i}\varepsilon_{\mathrm{f}}^{-1}\left[DU_1(kh_{\mathrm{d}}/2) - \Delta(kh_{\mathrm{d}}/2)\right]. \tag{3.18}$$

Now substitution of equation (3.16) into the boundary condition (3.14) at $x_2 = H/2$ yields

$$C_1^{\star} e^{kH/2} + C_2^{\star} e^{-kH/2} = 0. \tag{3.19}$$

Finally, by solving equations (3.18) and (3.19) we obtain the two constants $C_1^{\star}$, $C_2^{\star}$ as

$$\left.\begin{aligned} C_1^{\star} &= \frac{\mathrm{i}\left[DU_1(kh_{\mathrm{d}}/2) - \Delta(kh_{\mathrm{d}}/2)\right] e^{kh_{\mathrm{d}}/2}}{\varepsilon_{\mathrm{f}}\left(e^{kh_{\mathrm{d}}} + e^{kH}\right)} \\ \text{and} \quad C_2^{\star} &= -\frac{\mathrm{i}\left[DU_1(kh_{\mathrm{d}}/2) - \Delta(kh_{\mathrm{d}}/2)\right] e^{k(2H+h_{\mathrm{d}})/2}}{\varepsilon_{\mathrm{f}}\left(e^{kh_{\mathrm{d}}} + e^{kH}\right)}. \end{aligned}\right\} \tag{3.20}$$

Using equations (2.3), (3.2), (3.12), (3.13) and (3.16)–(3.20), we write the remaining interfacial conditions $(3.11)_{1,2,4}$ in an impedance form, as

$$\mathbf{S}(h_{\mathrm{d}}/2) = \mathrm{i}\,\mathbf{Z}_{+}^{\star}\mathbf{U}(h_{\mathrm{d}}/2), \tag{3.21}$$

where

$$\mathbf{Z}_{+}^{\star} = \varepsilon_{\mathrm{f}}^{-1}\begin{bmatrix} D^2\tanh\left[k(H-h_{\mathrm{d}})/2\right] & -\mathrm{i}D^2/2 & -D\tanh\left[k(H-h_{\mathrm{d}})/2\right] \\ \mathrm{i}D^2/2 & 0 & -\mathrm{i}D \\ -D\tanh\left[k(H-h_{\mathrm{d}})/2\right] & \mathrm{i}D & \tanh\left[k(H-h_{\mathrm{d}})/2\right] \end{bmatrix} \tag{3.22}$$

is a surface impedance matrix and $\mathbf{S}(h_{\mathrm{d}}/2)$ and $\mathbf{U}(h_{\mathrm{d}}/2)$ are the generalized displacement and traction vectors at the face $x_2 = h_{\mathrm{d}}/2$, respectively.

Similarly, the incremental electric potential $\dot{\phi}^{\star}$ for the silicone oil occupying the region $-h_{\mathrm{d}}/2 \ge x_2 \ge -H/2$ and satisfying the Laplace equation (3.15) has the form

$$\dot{\phi}_{-}^{\star}(x_1, x_2) = k^{-1}\left(C_3^{\star} e^{kx_2} + C_4^{\star} e^{-kx_2}\right) e^{\mathrm{i}kx_1}, \tag{3.23}$$

where $C_3^{\star}$ and $C_4^{\star}$ are constants, which can be determined similarly to $C_3^{\star}$ and $C_4^{\star}$, as

$$\left.\begin{aligned} C_3^{\star} &= \frac{\mathrm{i}\left[DU_1(-kh_{\mathrm{d}}/2) - \Delta(-kh_{\mathrm{d}}/2)\right] e^{k(2H+h_{\mathrm{d}})/2}}{\varepsilon_{\mathrm{f}}\left(e^{kh_{\mathrm{d}}} + e^{kH}\right)} \\ \text{and} \quad C_4^{\star} &= -\frac{\mathrm{i}\left[DU_1(-kh_{\mathrm{d}}/2) - \Delta(-kh_{\mathrm{d}}/2)\right] e^{kh_{\mathrm{d}}/2}}{\varepsilon_{\mathrm{f}}\left(e^{kh_{\mathrm{d}}} + e^{kH}\right)}. \end{aligned}\right\} \tag{3.24}$$

The interfacial conditions on the plate's face at $x_2 = -h_d/2$ can then be rewritten as

$$\mathbf{S}(-kh_d/2) = \mathrm{i}\mathbf{Z}^{\star}_{-}\mathbf{U}(-kh_d/2), \tag{3.25}$$

where

$$\mathbf{Z}^{\star}_{-} = \varepsilon_f^{-1}\begin{bmatrix} -D^2\tanh\left[k\left(H-h_d\right)/2\right] & -\mathrm{i}D^2/2 & D\tanh\left[k\left(H-h_d\right)/2\right] \\ \mathrm{i}D^2/2 & 0 & -\mathrm{i}D \\ D\tanh\left[k\left(H-h_d\right)/2\right] & \mathrm{i}D & -\tanh\left[k\left(H-h_d\right)/2\right] \end{bmatrix} \tag{3.26}$$

is a surface impedance matrix and $\mathbf{S}(-kh_d/2)$ and $\mathbf{U}(-kh_d/2)$ are the generalized displacement and traction vectors on the face $x_2 = -h_d/2$, respectively.

Combining equations (3.7), (3.21) and (3.25) gives

$$\begin{bmatrix} \mathbf{S}(kh/2) \\ \mathbf{S}(-kh/2) \end{bmatrix} = \mathrm{i}\begin{bmatrix} \mathbf{Z}^{\star}_{+} & \mathbf{0} \\ \mathbf{0} & \mathbf{Z}^{\star}_{-} \end{bmatrix}\begin{bmatrix} \mathbf{U}(kh/2) \\ \mathbf{U}(-kh/2) \end{bmatrix}$$

$$= \mathrm{i}\begin{bmatrix} \mathbf{Z}^{\star}_{+} & \mathbf{0} \\ \mathbf{0} & \mathbf{Z}^{\star}_{-} \end{bmatrix}\begin{bmatrix} \eta_1^{(1)}E_1^- & \eta_1^{(2)}E_2^- & \eta_1^{(3)}E_3^- & \eta_1^{(4)}E_1^+ & \eta_1^{(5)}E_2^+ & \eta_1^{(6)}E_3^+ \\ \eta_2^{(1)}E_1^- & \eta_2^{(2)}E_2^- & \eta_2^{(3)}E_3^- & \eta_2^{(4)}E_1^+ & \eta_2^{(5)}E_2^+ & \eta_2^{(6)}E_3^+ \\ \eta_3^{(1)}E_1^- & \eta_3^{(2)}E_2^- & \eta_3^{(3)}E_3^- & \eta_3^{(4)}E_1^+ & \eta_3^{(5)}E_2^+ & \eta_3^{(6)}E_3^+ \\ \eta_1^{(1)}E_1^+ & \eta_1^{(2)}E_2^+ & \eta_1^{(3)}E_3^+ & \eta_1^{(4)}E_1^- & \eta_1^{(5)}E_2^- & \eta_1^{(6)}E_3^- \\ \eta_2^{(1)}E_1^+ & \eta_2^{(2)}E_2^+ & \eta_2^{(3)}E_3^+ & \eta_2^{(4)}E_1^- & \eta_2^{(5)}E_2^- & \eta_2^{(6)}E_3^- \\ \eta_3^{(1)}E_1^+ & \eta_3^{(2)}E_2^+ & \eta_3^{(3)}E_3^+ & \eta_3^{(4)}E_1^- & \eta_3^{(5)}E_2^- & \eta_3^{(6)}E_3^- \end{bmatrix}\begin{bmatrix} c_1 \\ c_2 \\ c_3 \\ c_4 \\ c_5 \\ c_6 \end{bmatrix}. \tag{3.27}$$

The decoupled bifurcation equations of the plate are then obtained from simple algebraic manipulations [40] of equations (3.8) and (3.27). Considering antisymmetric modes only, we find

$$\begin{vmatrix} P_{11} & P_{12} & P_{13} \\ P_{21} & P_{22} & P_{23} \\ P_{31} & P_{32} & P_{33} \end{vmatrix} = 0, \tag{3.28}$$

where

$$\left.\begin{aligned} P_{1j} &= \eta_4^{(j)} - \frac{D}{2\varepsilon_f}\left\{D\eta_2^{(j)} + 2\mathrm{i}\left(-D\eta_1^{(j)} + \eta_3^{(j)}\right)\tanh\left[k(H-h_d)/2\right]\tanh(p_j kh_d/2)\right\}, \\ P_{2j} &= \left[\eta_5^{(j)} + \frac{D}{2\varepsilon_f}\left(D\eta_1^{(j)} - 2\eta_3^{(j)}\right)\right]\tanh(p_j kh_d/2) \\ \text{and}\quad P_{3j} &= \eta_6^{(j)} + \frac{1}{\varepsilon_f}\left\{D\eta_2^{(j)} + \mathrm{i}\left(-D\eta_1^{(j)} + \eta_3^{(j)}\right)\tanh\left[k(H-h_d)/2\right]\tanh(p_j kh_d/2)\right\}. \end{aligned}\right\}$$

Equation (3.28) is the *bifurcation criterion for the antisymmetric wrinkling mode of instability*, which always occurs first [21,26,35].

4. Numerical results for neo-Hookean dielectric plates

Here we specialize the theory presented in §3 to equi-biaxial deformations ($\lambda_1 = \lambda_3 = \lambda$ and $s_1 = s_3 = s$) of a *neo-Hookean electro-elastic* plate. Full details are given in appendix A. The electronic supplementary material contains all the Mathematica codes of the numerical calculations.

(a) Static response

The nonlinear response of an immersed neo-Hookean electro-elastic plate subject to a biaxial deformation is given in terms of the non-dimensional in-plane nominal stresses $\bar{s}_1 = s_1/\mu$,

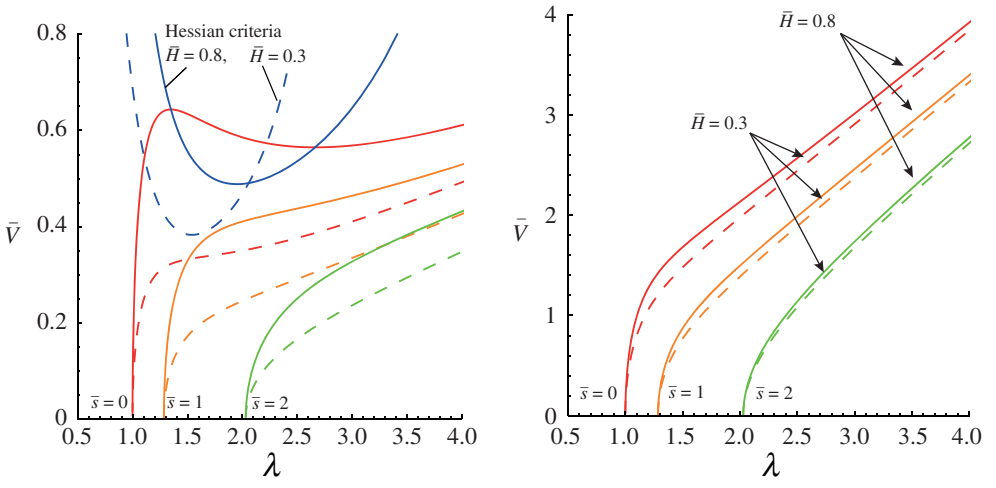

Figure 2. The continuous and dashed curves represent the nonlinear responses of a neo-Hookean electro-elastic plate immersed in silicone oil, for $\bar{H} = 0.8$ and $\bar{H} = 0.3$, respectively. The non-dimensionalized values of the equi-biaxial in-plane stress are $\bar{s} = 0, 1, 2$ and correspond to the red, orange and green curves, respectively. The panel on the left shows the Hessian criterion and the loading curves for a permittivity ratio $\bar{\varepsilon} = 0.1$. The panel on the right depicts the $\bar{V}$–λ curves for $\bar{\varepsilon} = 0.6$. The Hessian criteria curves do not cross any of the loading curves and are therefore not included in the latter. (Online version in colour.)

$\bar{s}_2 = s_2/\mu$ and of the electric potential in appendix A (see equations (A 3) and (A 4)). Specializing to equi-biaxial deformation, i.e. $\bar{s}_1 = \bar{s}_2 = \bar{s}$ and $\lambda_1 = \lambda_3 = \lambda$, we obtain

$$\bar{V} = \left[\bar{H}(1-\bar{\varepsilon}) + \bar{\varepsilon}\lambda^2\right]\sqrt{\frac{(\bar{s}-\lambda)\lambda^5 + 1}{(\bar{\varepsilon}-1)\lambda^8}}, \tag{4.1}$$

where $\bar{V} = (V/H)\sqrt{\varepsilon_\mathrm{d}/\mu}$ is a non-dimensional measure of the applied voltage, μ is the shear modulus of the solid in the absence of voltage, $\bar{H} = H_\mathrm{d}/H$ and $\bar{\varepsilon} = \varepsilon_\mathrm{d}/\varepsilon_\mathrm{f}$ are the ratios of the initial plate thickness to the distance of the electrodes and of the plate permittivity to that of the silicone oil, respectively. The voltage-induced stretch of the plate λ_V is then obtained from equation (4.1) for $\bar{s} = 0$.

It is well established that a pull-in instability of a neo-Hookean dielectric plate may be triggered when the nonlinear $\bar{V}$–λ response curve reaches a peak point [4,41]. From equation (4.1), $\bar{s}$ corresponding to the peak point $\mathrm{d}\bar{V}/\mathrm{d}\lambda = 0$ is obtained as

$$\bar{s}_\mathrm{cr} = \frac{2\left[\bar{H}(\bar{\varepsilon}-1)\left(\lambda^6-4\right) + \bar{\varepsilon}\lambda^2\left(\lambda^6+2\right)\right]}{\lambda^5\left[3\bar{H}(\bar{\varepsilon}-1) + \bar{\varepsilon}\lambda^2\right]}. \tag{4.2}$$

Inserting equation (4.2) into equation (4.1) then yields the *Hessian criterion* as

$$\bar{V} = \sqrt{\frac{\left[\bar{H}(1-\bar{\varepsilon}) + \bar{\varepsilon}\lambda^2\right]^3\left(\lambda^6+5\right)}{(\bar{\varepsilon}-1)\left[3\bar{H}(\bar{\varepsilon}-1) + \bar{\varepsilon}\lambda^2\right]\lambda^8}}. \tag{4.3}$$

Equations (4.1) and (4.3) show that the response of the electro-elastic plate depends on the values of $\bar{H}$ and $\bar{\varepsilon}$. In particular, from equation (4.1) we can see that when $\bar{\varepsilon} = 1$, the in-plane nominal stress $\bar{s}$ is not influenced by $\bar{V}$ and the plate deformation is independent of the electric field. When $\bar{\varepsilon} = 0$, $H_\mathrm{d} = H$, equation (4.1) recovers the equation governing the static deformation of DE plates with no exterior electric field, and (4.3) recovers its associated Hessian criterion [4].

The left panel in figure 2 displays the behaviour of an electro-elastic neo-Hookean plate immersed in silicone oil with relative permittivity $\bar{\varepsilon} = 0.1$, for relative thickness values $\bar{H} = 0.3$

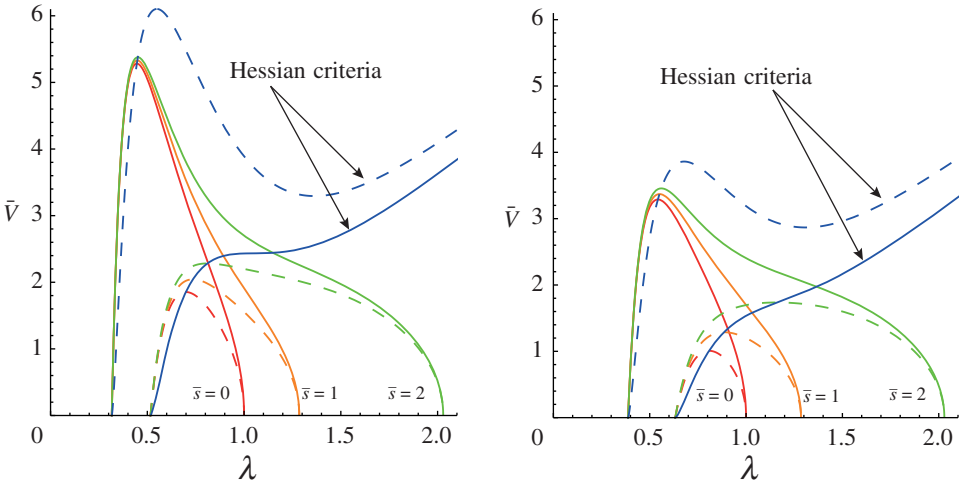

Figure 3. The Hessian criterion and the nonlinear response curves of an immersed neo-Hookean electro-elastic plate with $\bar{H}=0.8$ and $\bar{H}=0.3$ are depicted by continuous and dashed curves, respectively. The equi-biaxial in-plane stresses, in non-dimensionalized form, are $\bar{s}=0,1,2$ and correspond, respectively, to the red, orange and green curves. The panel on the left represents the behaviour for $\bar{\varepsilon}=1.5$, the one on the right for $\bar{\varepsilon}=2$. (Online version in colour.)

(dashed curves) and $\bar{H}=0.8$ (solid curves). The non-dimensional in-plane pre-stresses $\bar{s}=0,1,2$ are considered, shown by red, orange and green curves, respectively. The curves corresponding to the Hessian criterion when $\bar{H}=0.3$ (dashed curve) and $\bar{H}=0.8$ (solid curve) are also displayed. As an electric field is applied, the stretch increases until a homogeneous pull-in instability occurs when the loading curve crosses the Hessian criterion. This occurs, for example, for $\bar{s}=0$ and $\bar{H}=0.8$, but not for $\bar{s}=0$ and $\bar{H}=0.3$. The panel on the right shows the results corresponding to $\bar{\varepsilon}=0.6$. In that case, the curves corresponding to the Hessian criteria do not intersect any of the three loading curves and for the sake of clarity are therefore not shown. The figures show that the pull-in instability can be suppressed by increasing the value of $\bar{\varepsilon}$ and/or reducing the value of $\bar{H}$. They also show that increasing values of $\bar{\varepsilon}$ and/or $\bar{H}$ stiffen the response, i.e. a larger potential is needed to achieve the same deformation.

The dependence of the in-plane stretch λ on the non-dimensional form of the electric potential $\bar{V}$ for values of $\bar{\varepsilon}=1.5,2$ is shown in figure 3. In contrast to the behaviour depicted in figure 2, the application of an electric field now induces a *lateral contraction of the plate*, as λ decreases with increasing $\bar{V}$. The initial response is monotonic until a critical point is reached when $\mathrm{d}\bar{V}/\mathrm{d}\lambda=0$. At this point the Hessian criterion indicates a *'pull-out' instability*, with a uniform increase in thickness accompanied by large lateral contraction. The system becomes more stable for lower values of $\bar{H}$ and $\bar{\varepsilon}$.

(b) Wrinkling analysis

Specializing equation (A 7) to equi-biaxial deformation, and using equation (A 3), gives the wrinkling criterion for the immersed plate as

$$\bar{V}=\left[\bar{H}\left(1-\bar{\varepsilon}\right)+\bar{\varepsilon}\lambda^2\right]\sqrt{\bar{\varepsilon}\tanh\left[\pi\left(\bar{H}\lambda^2-1\right)H_{\mathrm{d}}/\left(\lambda^2\mathcal{L}\right)\right]+\coth\left[\pi H_{\mathrm{d}}/\left(\lambda^2\mathcal{L}\right)\right]}$$
$$\sqrt{\frac{\left(\lambda^6+1\right)^2\tanh\left[\pi H_{\mathrm{d}}/\left(\lambda^2\mathcal{L}\right)\right]-4\lambda^3\tanh\left(\pi\lambda H_{\mathrm{d}}/\mathcal{L}\right)}{\lambda^8\left(\bar{\varepsilon}-1\right)^2\left(\lambda^6-1\right)}}. \tag{4.4}$$

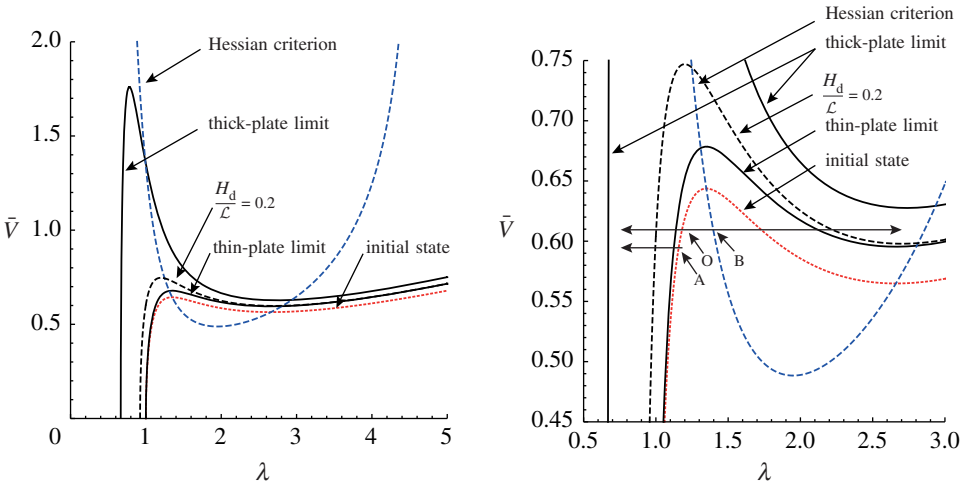

Figure 4. The wrinkling behaviour of an immersed neo-Hookean electro-elastic plate with $\bar{H} = 0.8$ and $\bar{\varepsilon} = 0.1$. The solid curves correspond to the thin- and thick-plate limits, the dashed black curve represents the behaviour when $H_d/\mathcal{L} = 0.2$. The initial state is obtained by the application of an electric potential with $\bar{s} = 0$ and is depicted by a red dotted curve. It shows that an exterior electric field has a stabilizing effect. The Hessian criterion indicates the onset of a pull-in instability and is depicted by the blue dashed curve. (Online version in colour.)

The wrinkling criteria for thin and thick plates are obtained by evaluating (4.4) when $H_d/\mathcal{L} \to 0$ and $H_d/\mathcal{L} \to \infty$, respectively. For thin plates we have

$$\bar{V} = \left[\bar{H}(1-\bar{\varepsilon}) + \bar{\varepsilon}\lambda^2\right]\sqrt{\frac{\lambda^6 - 1}{(\bar{\varepsilon}-1)^2\lambda^8}}, \tag{4.5}$$

while for thick plates we have

$$\bar{V} = \left[\bar{H}(1-\bar{\varepsilon}) + \bar{\varepsilon}\lambda^2\right]\sqrt{\frac{(\bar{\varepsilon}+1)\left(\lambda^9 + \lambda^6 + 3\lambda^3 - 1\right)}{\lambda^8(\bar{\varepsilon}-1)^2\left(\lambda^3+1\right)}}. \tag{4.6}$$

Note that unlike the results in [21] (no exterior electrical field), the loading curve $\bar{V}$–λ with no in-plane pre-stresses is not equivalent to the wrinkling limit for plates with vanishing thickness.

Figures 4 and 5 summarize the response of an immersed neo-Hookean electro-elastic plate with relative permittivity $\bar{\varepsilon} = 0.1$ and thickness ratio $\bar{H} = 0.8$. Figure 4, in particular, depicts the Hessian criterion (4.3), the wrinkling criterion (4.4) for $H_d/\mathcal{L} = 0.2$ and the criteria (4.5), (4.6) for thin and thick plates, respectively. The initial state, depicted by a red dashed curve is obtained from (4.1) with $\bar{s} = 0$. It shows that the electric field generated by $\bar{V}$ induces a reduction in thickness and by incompressibility, an equi-biaxial stretch λ. Consider, for example, the initial state O of a thin plate with $H_d/\mathcal{L} \to 0$ defined by point O in the right panel in figure 4. It shows that an in-plane biaxial compression $\bar{s} < 0$ is required to induce the wrinkled state. This differs from the behaviour of DE plates shown in figure 1*a* by Su *et al.* [21], where a thin plate buckles immediately upon the application of a small compressive mechanical load. Alternatively, an in-plane tensile stress deforms the plate from the initial state O to point B where the Hessian criterion is met, resulting in uncontrolled uniform thinning. Of interest is the initial state defined by point A and corresponding to an electric potential $\bar{V} = 0.59$. It shows that wrinkling occurs for in-plane contraction with the magnitude a function of the ratio $H_d/\mathcal{L}$. Maintaining $\bar{V} = 0.59$ constant, an in-plane extension of sufficient magnitude will satisfy the Hessian criterion but wrinkling in tension will not occur.

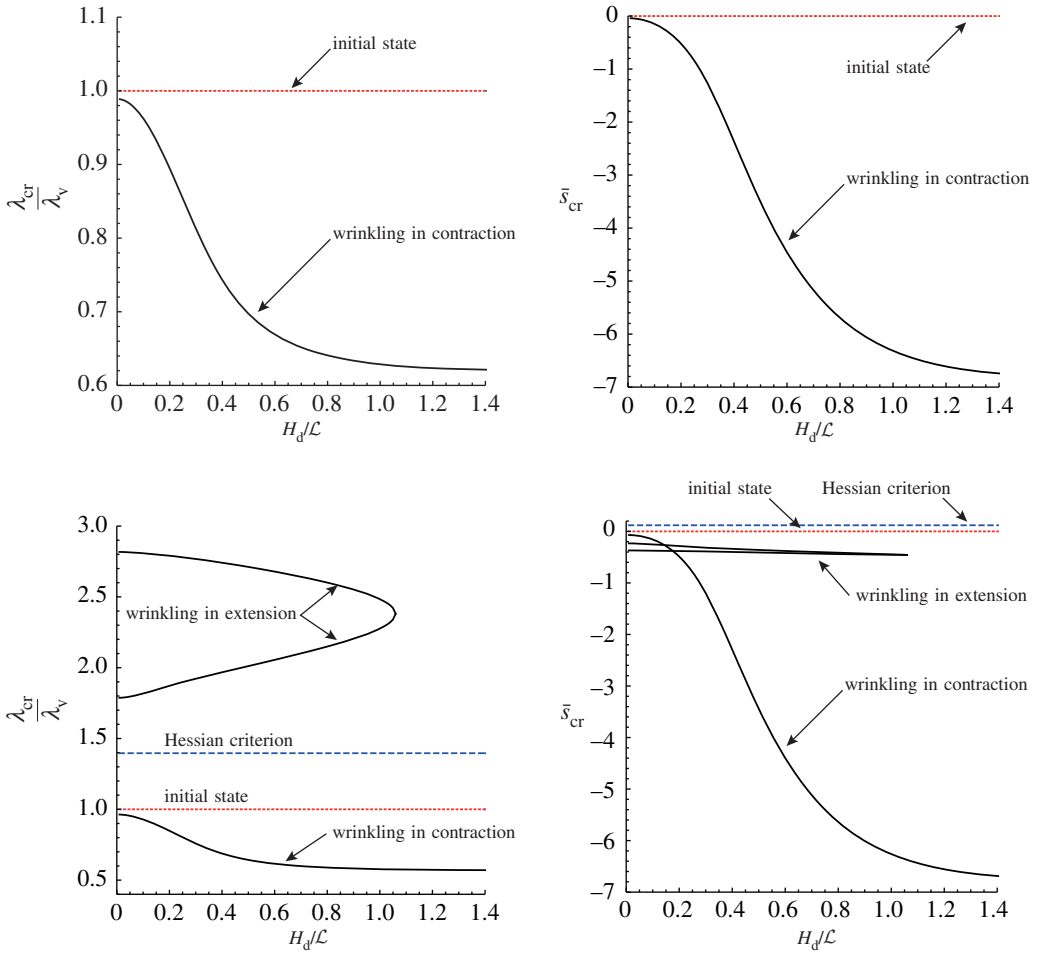

Figure 5. The upper and lower panels show the ratio λ_{cr}/λ_V and the non-dimensional in-plane critical stress $\bar{s}_{cr}$ as a function of the thickness to wavelength ratio $H_d/\mathcal{L}$ for the electric potentials $\bar{V} = 0.5$ and $\bar{V} = 0.61$, respectively (plate immersed in silicone oil). The solid curves represent the wrinkling behaviour in contraction and extension. The red dotted and blued dashed curves show the initial state and the Hessian criterion, respectively. (Online version in colour.)

Figure 5 shows the ratio λ_{cr}/λ_V and the non-dimensional in-plane critical stress $\bar{s}_{cr}$ as a function of the thickness to wavelength ratio $H_d/\mathcal{L}$ for the electric potentials $\bar{V} = 0.5$ and $\bar{V} = 0.61$ using solid curves to indicate wrinkling (here λ_{cr} is the critical stretch of wrinkling). In particular, for $\bar{V} = 0.5$ wrinkling occurs in compression only with in-plane contraction and critical stress increasing with $H_d/\mathcal{L}$. For an electric potential $\bar{V} = 0.61$ the behaviour in compression is similar; however, the behaviour in extension is different, with equi-biaxial deformation of sufficient magnitude inducing uniform thinning when the Hessian criterion is met. For increasing values of λ, wrinkling in extension occurs.

The initial state, the wrinkling behaviour for a plate with $H_d/\mathcal{L} = 0.2$, and the thin- and thick-plate limits are shown in figure 6 for $\bar{\varepsilon} = 0.3, 0.6$ and for $\bar{H} = 0.3, 0.8$. The initial state for a potential difference $\bar{V}$ is defined by stable biaxial stretch λ with magnitude influenced by $\bar{\varepsilon}$ and $\bar{H}$. Take, for example, the initial state defined by $\lambda = 2$. The two panels on the left show that the required potential difference increases with $\bar{\varepsilon}$. On the other hand, the two panels on the right show that a change in $\bar{H}$ does not significantly influence the value of $\bar{V}$ to obtain the initial deformation $\lambda = 2$. A subsequently applied in-plane biaxial stress $\bar{s} < 0$, with $\bar{V}$ constant, induces wrinkling

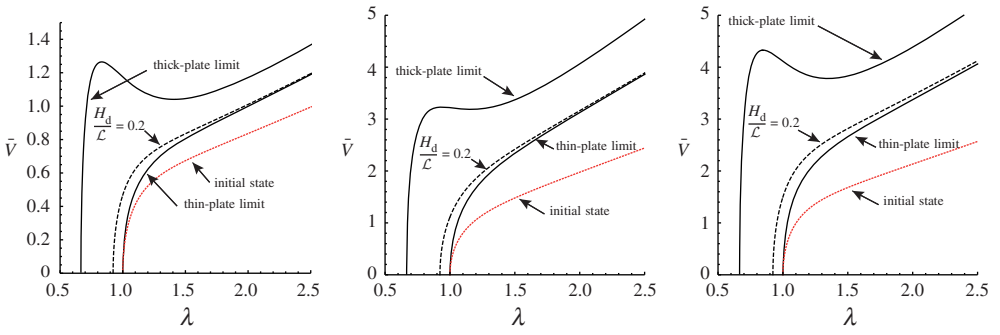

Figure 6. Dependence of the non-dimensional electric potential $\bar{V}$ on the in-plane stretch λ for values of $\bar{\varepsilon} = 0.3, 0.6$ and $\bar{H} = 0.3, 0.8$. Specifically, the panel on the left shows the wrinkling behaviour and the initial state for $\bar{\varepsilon} = 0.3$, $\bar{H} = 0.3$, the centre panel corresponds to $\bar{\varepsilon} = 0.6$, $\bar{H} = 0.3$ and the results on the right to $\bar{\varepsilon} = 0.6$, $\bar{H} = 0.8$. (Online version in colour.)

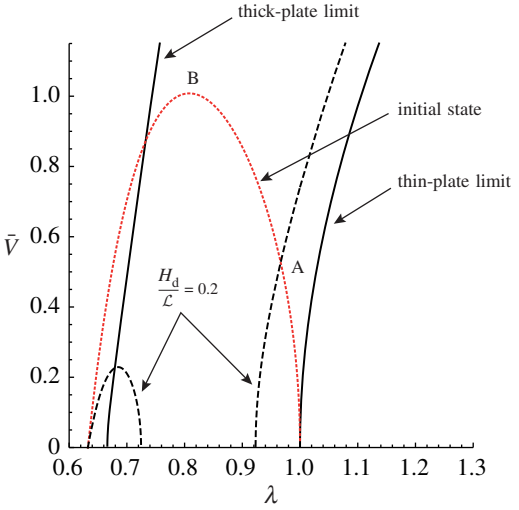

Figure 7. The $\bar{V}$–λ loading curves and the initial state of an immersed neo-Hookean electro-elastic plate for permittivity and thickness ratios $\bar{\varepsilon} = 2$ and $\bar{H} = 0.8$, respectively. The solid curves depict the behaviour for the thin- and thick-plate limits, the dashed curve corresponds to $H_d/\mathcal{L} = 0.2$ and the dotted red curve represents the initial state when $\bar{s} = 0$. (Online version in colour.)

with the amount of contraction increasing with $H_d/\mathcal{L}$. Alternatively, to keep $\lambda = 2$ constant when the potential $\bar{V}$ is increased requires an in-plane stress $\bar{s} < 0$. The graphs show that the increase in $\bar{V}$ inducing wrinkling, for $\lambda = 2$ constant, depends on $\bar{\varepsilon}$ and that the influence of $\bar{H}$ is minor.

Figures 7 illustrates the $\bar{V}$–λ loading curves of an immersed electro-elastic plate for a relative permittivity $\bar{\varepsilon} = 2$ and for a ratio of plate thickness to electrode distance $\bar{H} = 0.8$. In addition to the wrinkling behaviour for thin- and thick-plate limits and for $H_d/\mathcal{L} = 0.2$, figure 7 also depicts the initial state obtained by a potential difference at the electrodes with $\bar{s} = 0$. As already shown in figure 3, the potential difference at the electrodes, with $\bar{s} = 0$, induces an increase in plate thickness and by incompressibility a biaxial contraction $\lambda < 1$. The initial state of a plate with $H_d/\mathcal{L} = 0.2$, for example, buckles at point A and can be stabilized by the application of an in-plane biaxial tension $\bar{s} > 0$. For plates with $H_d/\mathcal{L} > 0.2$ and with the electric potential constant and equal to the one indicated by point A, an in-plane compression $\bar{s} < 0$ is necessary to induce a wrinkled configuration. The electric potential $\bar{V}$ corresponding to the initial state B induces a pull-out instability in the plate (see figure 3).

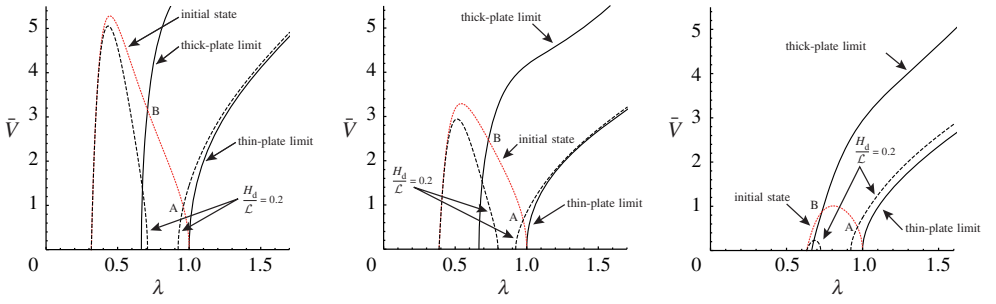

Figure 8. The panel on the left shows the initial state and the dependence of the non-dimensional electric potential $\bar{V}$ on the in-plane stretch λ for values of $\bar{\varepsilon} = 1.5$ and $\bar{H} = 0.3$. The panel in the centre is obtained when $\bar{\varepsilon} = 2$ and $\bar{H} = 0.3$ and the results on the right correspond to $\bar{\varepsilon} = 2$ and $\bar{H} = 0.8$. (Online version in colour.)

The wrinkling behaviour for the thin- and thick-plate limits and for $H_d/\mathcal{L} = 0.2$ as well as the initial state are shown in figure 8 for $\bar{\varepsilon} = 1.5, 2$ and $\bar{H} = 0.3, 0.8$. The main difference from the results in figure 6 is the use of larger values of $\bar{\varepsilon}$. The results indicate that increasing the potential difference at the electrodes, with in-plane stress $\bar{s} = 0$, induces wrinkles at point A for a plate with $H_d/\mathcal{L} = 0.2$ and at point B for the thick-plate limit. In particular, consider the initial state defined by a biaxial stretch $\lambda = 0.8$. The three panels show a reduction in the electric potential with increased values of $\bar{\varepsilon}$ and $\bar{H}$. An in-plane contraction or extension, superposed on the initial state $\lambda = 0.8$, with $\bar{V}$ constant, induces a wrinkled configuration depending on the specific value of H_d/L. Figure 8 also shows that an in-plane tension $\bar{s} > 0$ must be superposed to keep the stretch $\lambda = 0.8$ constant for increasing values of $\bar{V}$.

5. Conclusion

(a) Results

This paper analyses the influence of an external field on the stability (Hessian criterion and wrinkling bifurcation) of an electro-elastic plate subject to an in-plane equi-biaxial contraction or extension. The plate is immersed in a tank filled with silicone oil with the electric field generated by two fixed rigid electrodes placed on top and bottom of the tank. Provided the plate thickness is small compared to the lateral dimensions, which we assume to be the case, the electric field within the plate can be taken as uniform. We can then obtain the equations governing the nonlinear response in terms of the non-dimensionalized in-plane nominal stress $\bar{s}$ and the potential difference $\bar{V}$.

We find that the response of the immersed plate depends on the values of $\bar{\varepsilon} = \varepsilon_d/\varepsilon_f$, the ratio of plate permittivity to that of the silicone oil, of $H_d/\mathcal{L}$, the ratio of the plate thickness to the wavelength, and of $\bar{H} = H_d/H$, the ratio of the initial plate thickness to the distance of the electrodes. For example, an increase in the electric potential induces a thinning of the plate and an accompanied lateral expansion when $\bar{\varepsilon} = 0.1, 0.6$, similar to the behaviour in the absence of external field. But for the values $\bar{\varepsilon} = 1.5, 2.0$, the potential $\bar{V}$ generates an *increase in plate thickness* and therefore a lateral contraction.

First, we use the Hessian criterion to signal electro-mechanical instability. When the electric field induces uniform thinning of the plate accompanied by a sudden increase in the in-plane stretch λ, we have the well-known *pull-in instability*. However, the Hessian criterion also identifies a *pull-out instability*, when the plate thickens with the electric field.

Then we derive incremental forms of the governing equations and boundary conditions in the Stroh form and obtain the explicit bifurcation conditions for antisymmetric and symmetric modes.

We focus on a neo-Hookean electro-elastic material with a deformation-independent permittivity to illustrate the results.

For the immersed plate, the curve showing the electric potential $\bar{V}$ versus the in-plane stretch λ, with pre-stress $\bar{s}=0$, no longer represents the wrinkling limit for plates with vanishing thickness. Wrinkling in contraction or extension can now be delayed or suppressed by adjusting the values of the ratios $\bar{H}$, $\bar{\varepsilon}$ and $H_{\mathrm{d}}/\mathcal{L}$. The activation protocol analysed in this problem can therefore be used to optimize the design of electro-elastic sensors and actuators.

(b) Limitations

In this paper, we consider a two-dimensional incremental wrinkling deformation superposed upon a large equi-biaxial deformation. It is two-dimensional in the sense that the incremental fields depend on two space variables only, x_1 and x_2. It follows that on the plate surfaces at $x_2=\pm H_{\mathrm{d}}/2$ we see a one-dimensional sinusoidal pattern emerge. In general, the deformed plate may buckle in either a one- or two-dimensional wrinkling pattern, depending on the material properties and loading conditions.

From a practical viewpoint, we assumed that the incremental loading and boundary conditions superposed on the equi-biaxial deformed configuration cannot be exactly the same, and that the wrinkles' front is normal to the direction of the slightly larger load. Here we chose x_1 as the normal to the wrinkles' front, although we could have equally chosen any other direction in the (x_1,x_3) plane (and obtained the same critical thresholds). To predict a two-dimensional wrinkling pattern, a three-dimensional incremental analysis is required; see Su *et al.* [42] for an example.

Note that we focused on the *static* wrinkling behaviour of electro-elastic plates, and that viscosity [43] of the conductive fluid was not considered.

We also studied the Hessian instability, but did not look at other instability modes such as, for example, the necking instability, see Fu *et al.* [44], and left aside the possibility of an electric breakdown of the DE plate. For a detailed discussion on that latter topic, the interested readers are referred to recent papers by Su *et al.* [21,41].

Data accessibility. This article has no additional data.

Authors' contributions. Y.S.: conceptualization, derivation of the formulae, numerical analysis, writing. W.C.: derivation of the formulae, supervision, writing. L.D.: numerical analysis, writing. M.D.: conceptualization, supervision, writing.

Competing interests. There is no conflict of interest.

Funding. This work was supported by a Government of Ireland Postdoctoral Fellowship from the Irish Research Council (grant no. GOIPD/2017/1208) and by the National Natural Science Foundation of China (grant no. 11621062). W.C. and Y.S. also acknowledge the support from the Shenzhen Scientific and Technological Fund for R&D (grant no. JCYJ20170816172316775).

Acknowledgements. M.D. thanks Zhejiang University for funding research visits to Hangzhou.

Appendix A. Stroh method for a neo-Hookean electro-elastic plate

We restrict attention to an incompressible neo-Hookean electro-elastic plate with underlying in-plane biaxial deformation λ_1, λ_3 and with out-of-plane stretch $\lambda_2=\lambda_1^{-1}\lambda_3^{-1}$. The Stroh method is used to derive the bifurcation equation and details are provided.

Following [21] and [35], we consider an incompressible neo-Hookean electro-elastic material with the energy function

$$W(\lambda_1,\lambda_3,E_0)=\frac{\mu}{2}\left(\lambda_1^2+\lambda_3^2+\lambda_1^{-2}\lambda_3^{-2}-3\right)-\frac{\varepsilon_{\mathrm{d}}}{2}\lambda_1^2\lambda_3^2E_0^2, \tag{A 1}$$

where μ is the shear modulus defined in the undeformed configuration and ε_{d} is the electric permittivity. Then, the explicit expressions of the coefficients in (3.4) are

$$a=\mu\lambda_1^2\left(1-\lambda_3^2\bar{E}_0^2\right),\quad b=\frac{\mu}{2}\left(\lambda_1^2+\lambda_1^{-2}\lambda_3^{-2}-\lambda_1^2\lambda_3^2\bar{E}_0^2\right),$$

$$c=\mu\lambda_1^{-2}\lambda_3^{-2},\quad d=\mu\lambda_1\lambda_3\bar{E}_0,\quad e=2d,\quad f=g=-\varepsilon_{\mathrm{d}}, \tag{A 2}$$

where $\bar{E}_0=E_0\sqrt{\varepsilon_{\mathrm{d}}/\mu}$ is the non-dimensional form of the nominal electric field in the plate.

(a) Static response

The nominal electric field component E_0 is obtained from equation (2.5) using the energy function (A 1). This component, in non-dimensional form, has the expression

$$\bar{E}_0=\frac{\bar{V}}{\bar{H}\,(1-\bar{\varepsilon})+\bar{\varepsilon}\lambda_1\lambda_3}, \tag{A 3}$$

where $\bar{V}=V\sqrt{\varepsilon_{\mathrm{d}}/\mu}/H$ is the non-dimensionalized form of the electric potential, $\bar{H}=H_{\mathrm{d}}/H$ is the ratio of the initial plate thickness to the distance of the electrodes and $\bar{\varepsilon}=\varepsilon_{\mathrm{d}}/\varepsilon_{\mathrm{f}}$ denotes the ratio of the plate permittivity to that of the silicone oil.

For the neo-Hookean electro-elastic material (A 1), the expressions of the in-plane nominal stress components s_1, s_3 are obtained from (2.6) and (2.8). These are, in non-dimensionalized form

$$\bar{s}_1=\lambda_1-\lambda_1^{-3}\lambda_3^{-2}-(1-\bar{\varepsilon})\,\bar{E}_0^2\lambda_1\lambda_3^2,\quad \bar{s}_3=\lambda_3-\lambda_1^{-2}\lambda_3^{-3}-(1-\bar{\varepsilon})\,\bar{E}_0^2\lambda_1^2\lambda_3, \tag{A 4}$$

where $\bar{s}_i=s_i/\mu$ $(i=1,3)$.

(b) Wrinkling stability analysis

The eigenvalues are obtained by solving equation (3.6), which can be written in compact form as

$$p_1=-p_4=\lambda_1^2\lambda_3,\qquad p_2=-p_5=p_3=-p_6=1. \tag{A 5}$$

The component forms of the corresponding eigenvectors $\boldsymbol{\eta}^{(i)}, i=1,\ldots,6$, are

$$\boldsymbol{\eta}^{(1)}=\begin{bmatrix} 2\mathrm{i}\lambda_1^4\lambda_3^3 \\ -2\lambda_1^2\lambda_3^2 \\ 2\mathrm{i}\sqrt{\varepsilon_{\mathrm{d}}\mu}\lambda_1^5\lambda_3^4\bar{E}_0 \\ \mu\lambda_1^4\lambda_3^2\left[\lambda_3^2\bar{E}_0^2\,(\bar{\varepsilon}-2)-2\right]-2\mu \\ \mathrm{i}\mu\lambda_1^2\lambda_3\left(\lambda_1^4\lambda_3^4\bar{\varepsilon}\bar{E}_0^2-4\right) \\ 2\sqrt{\mu/\varepsilon_{\mathrm{d}}}\lambda_1^3\lambda_3^3\bar{E}_0 \end{bmatrix},$$

$$\boldsymbol{\eta}^{(2)}=\begin{bmatrix} 2\mathrm{i}\lambda_1^2\lambda_3^3 \\ -2\lambda_1^2\lambda_3^2 \\ 4\mathrm{i}\sqrt{\varepsilon_{\mathrm{d}}\mu}\lambda_1^3\lambda_3^3\bar{E}_0 \\ \mu\left(\lambda_1^4\lambda_3^4\bar{\varepsilon}\bar{E}_0^2-4\right) \\ \mathrm{i}\mu\lambda_1^4\lambda_3^2\left[\lambda_3^2\bar{E}_0^2\,(\bar{\varepsilon}+2)-2\right]-2\mu \\ 0 \end{bmatrix},$$

$$\boldsymbol{\eta}^{(3)}=\begin{bmatrix} 2\mathrm{i}\lambda_1^3\lambda_3^3\bar{E}_0 \\ 2\lambda_1^3\lambda_3^3\bar{E}_0 \\ \mathrm{i}\sqrt{\varepsilon_{\mathrm{d}}\mu}\lambda_1^4\lambda_3^2\left[2-\lambda_3^2\bar{E}_0^2\,(\bar{\varepsilon}-2)\right]+2\mathrm{i}\sqrt{\varepsilon_{\mathrm{d}}\mu} \\ -2\mu\lambda_1\lambda_3\bar{E}_0\left(\lambda_1^4\lambda_3^4\bar{E}_0^2-\lambda_1^4\lambda_3^2+1\right) \\ 0 \\ \sqrt{\varepsilon_{\mathrm{d}}\mu}\lambda_1^4\lambda_3^2\left[\lambda_3^2\bar{E}_0^2\,(\bar{\varepsilon}+2)-2\right]-2\sqrt{\varepsilon_{\mathrm{d}}\mu} \end{bmatrix},$$

$$\boldsymbol{\eta}^{(4)}=\left(\boldsymbol{\eta}^{(1)}\right)^*,\quad \boldsymbol{\eta}^{(5)}=\left(\boldsymbol{\eta}^{(2)}\right)^*,\quad \boldsymbol{\eta}^{(6)}=\left(\boldsymbol{\eta}^{(3)}\right)^*. \tag{A 6}$$

The wrinkling criterion for antisymmetric modes is obtained from (3.28) and has the explicit non-dimensional form

$$\bar{E}_0 = \sqrt{\bar{\varepsilon}\tanh\left[\pi\left(\bar{H}-\lambda_1^{-1}\lambda_3^{-1}\right)H_{\mathrm{d}}/\mathcal{L}\right]+\coth\left(\pi\lambda_1^{-1}\lambda_3^{-1}H_{\mathrm{d}}/\mathcal{L}\right)}\sqrt{\frac{\left(\lambda_1^4\lambda_3^2+1\right)^2\tanh\left(\pi\lambda_1^{-1}\lambda_3^{-1}H_{\mathrm{d}}/\mathcal{L}\right)-4\lambda_1^2\lambda_3\tanh\left(\pi\lambda_1 H_{\mathrm{d}}/\mathcal{L}\right)}{\lambda_1^4\lambda_3^4\left(\bar{\varepsilon}-1\right)^2\left(\lambda_1^4\lambda_3^2-1\right)}}. \tag{A 7}$$

The thin- and thick-plate wrinkling criteria are obtained by evaluating (A 7) for $H/\mathcal{L}\to 0$ and $H/\mathcal{L}\to\infty$, respectively. In non-dimensional forms, these are given by

$$\bar{E}_0 = \sqrt{\frac{\lambda_1^4\lambda_3^2-1}{\lambda_1^4\lambda_3^4\left(\bar{\varepsilon}-1\right)^2}} \tag{A 8}$$

and

$$\bar{E}_0 = \sqrt{\frac{\left(\bar{\varepsilon}+1\right)\left[\lambda_1^2\lambda_3\left(\lambda_1^4\lambda_3^2+\lambda_1^2\lambda_3+3\right)-1\right]}{\lambda_1^4\lambda_3^4\left(\bar{\varepsilon}-1\right)^2\left(\lambda_1^2\lambda_3+1\right)}}. \tag{A 9}$$

Equation (A 7), using the connection (A 3) with $\bar{V}=0$, identifies a configuration where an antisymmetric wrinkling mode may exist for a purely elastic plate.

References

1. Bar-Cohen Y. 2004 *Electroactive polymer (EAP) actuators as artificial muscles: reality, potential, and challenges*, vol. 136. Bellingham, WA: SPIE Press.
2. Paul B, Pei QB. 2010 Advances in dielectric elastomers for actuators and artificial muscles. *Macromol. Rapid Commun.* **31**, 10–36. (doi:10.1002/marc.200900425)
3. Li Q, Yao FZ, Liu Y, Zhang G, Wang H, Wang Q. 2018 High-temperature dielectric materials for electrical energy storage. *Annu. Rev. Mater. Res.* **48**, 219–243. (doi:10.1146/annurev-matsci-070317-124435)
4. Zhao XH, Suo ZG. 2007 Method to analyze electromechanical stability of dielectric elastomers. *Appl. Phys. Lett.* **9**, 061921. (doi:10.1063/1.2768641)
5. Koh SJA, Keplinger C, Li T, Bauer S, Suo Z. 2011 Dielectric elastomer generators: how much energy can be converted? *IEEE ASME Trans. Mechatron.* **16**, 33–41. (doi:10.1109/TMECH.2010.2089635)
6. Che S, Lu T, Wang TJ. 2017 Electromechanical phase transition of a dielectric elastomer tube under internal pressure of constant mass. *Theor. Appl. Mech. Lett.* **7**, 121–125. (doi:10.1016/j.taml.2017.02.004)
7. Keplinger C, Kaltenbrunner M, Arnold N, Bauer S. 2010 Röntgen's electrode-free elastomer actuators without electromechanical pull-in instability. *Proc. Natl Acad. Sci. USA* **107**, 4505–4510. (doi:10.1073/pnas.0913461107)
8. Li B, Zhou JX, Chen HL. 2011 Electromechanical stability in charge-controlled dielectric elastomer actuation. *Appl. Phys. Lett.* **99**, 244101. (doi:10.1063/1.3670048)
9. Sun JY, Keplinger C, Whitesides GM, Suo ZG. 2014 Ionic skin. *Adv. Mater.* **26**, 7608–7614. (doi:10.1002/adma.201403441)
10. O'Halloran A, O'Malley F, McHugh P. 2008 A review on dielectric elastomer actuators, technology, applications, and challenges. *J. Appl. Phys.* **104**, 071101. (doi:10.1063/1.2981642)
11. Fukada E, Yasuda I. 1957 On the piezoelectric effect of bone. *J. Phys. Soc. Jpn.* **12**, 1158–1162. (doi:10.1143/JPSJ.12.1158)
12. Fukada E. 1968 Piezoelectricity in polymers and biological materials. *Ultrasonics* **6**, 229–234. (doi:10.1016/0041-624X(68)90132-7)
13. Pietak A, Levin M. 2016 Exploring instructive physiological signaling with the bioelectric tissue simulation engine. *Front. Bioeng. Biotechnol.* **4**, 00055. (doi:10.3389/fbioe.2016.00055)
14. Dorfmann L, Ogden RW. 2014 Nonlinear response of an electro-elastic spherical shell. *Int. J. Eng. Sci.* **85**, 163–174. (doi:10.1016/j.ijengsci.2014.09.001)

15. Bortot E. 2017 Analysis of multilayer electro-active spherical balloons. *J. Mech. Phys. Solids* **101**, 250–267. (doi:10.1016/j.jmps.2017.02.001)
16. Zhu J, Cai SQ, Suo ZG. 2010 Resonant behavior of a membrane of a dielectric elastomer. *Int. J. Solids Struct.* **47**, 3254–3262. (doi:10.1016/j.ijsolstr.2010.08.008)
17. Wang F, Lu TQ, Wang TJ. 2016 Nonlinear vibration of dielectric elastomer incorporating strain stiffening. *Int. J. Solids Struct.* **87**, 70–80. (doi:10.1016/j.ijsolstr.2016.02.030)
18. Jin XL, Wang Y, Huang ZL. 2017 On the ratio of expectation crossings of random-excited dielectric elastomer balloon. *Theor. Appl. Mech. Lett.* **7**, 100–104. (doi:10.1016/j.taml.2017.03.005)
19. Galich PI, Rudykh S. 2017 Shear wave propagation and band gaps in finitely deformed dielectric elastomer laminates: long wave estimates and exact solution. *J. Appl. Mech.* **84**, 091002. (doi:10.1115/1.4037159)
20. Yang SY, Zhao XH, Sharma P. 2017 Revisiting the instability and bifurcation behavior of soft dielectrics. *J. Appl. Mech.* **84**, 031008. (doi:10.1115/1.4035499)
21. Su YP, Broderick HC, Chen WQ, Destrade M. 2018 Wrinkles in soft dielectric plates. *J. Mech. Phys. Solids* **119**, 298–318. (doi:10.1016/j.jmps.2018.07.001)
22. Shmuel G. 2013 Electrostatically tunable band gaps in finitely extensible dielectric elastomer fiber composites. *Int. J. Solids Struct.* **50**, 680–686. (doi:10.1016/j.ijsolstr.2012.10.028)
23. Wu B, Zhang CZ. 2017 On guided circumferential waves in soft electroactive tubes under radially inhomogeneous biasing fields. *J. Mech. Phys. Solids* **99**, 116–145. (doi:10.1016/j.jmps.2016.11.004)
24. Dorfmann L, Ogden RW. 2020 Waves and vibrations in a finitely deformed electro-elastic circular cylindrical tube. *Proc. R. Soc. A* **476**, 20190701. (doi:10.1098/rspa.2019.0701)
25. Dorfmann A, Ogden RW. 2010 Nonlinear electro-elastostatics: incremental equations and stability. *Int. J. Eng. Sci.* **48**, 1–14. (doi:10.1016/j.ijengsci.2008.06.005)
26. Dorfmann L, Ogden RW. 2014 Instabilities of an electro-elastic plate. *Int. J. Eng. Sci.* **77**, 79–101. (doi:10.1016/j.ijengsci.2013.12.007)
27. Chen WQ, Dai HH. 2012 Waves in pre-stretched incompressible soft electro active cylinders: exact solution. *Acta Mech. Solida Sin.* **25**, 530–541. (doi:10.1016/S0894-9166(12)60047-0)
28. Su YP, Wang HM, Zhang CL, Chen WQ. 2016 Propagation of non-axisymmetric waves in an infinite soft electroactive hollow cylinder under uniform biasing fields. *Int. J. Solids Struct.* **81**, 262–273. (doi:10.1016/j.ijsolstr.2015.12.003)
29. Su YP, Zhou WJ, Chen WQ, Lü CF. 2016 On buckling of a soft incompressible electroactive hollow cylinder. *Int. J. Solids Struct.* **97–98**, 400–416. (doi:10.1016/j.ijsolstr.2016.07.008)
30. Díaz-Calleja R, Sanchis MJ, Riande E. 2009 Effect of an electric field on the bifurcation of a biaxially stretched incompressible slab rubber. *Eur. Phys. J. E* **30**, 417–426. (doi:10.1140/epje/i2009-10541-4)
31. Wang QM, Zhang L, Zhao XH. 2011 Creasing to cratering instability in polymers under ultrahigh electric fields. *Phys. Rev. Lett.* **106**, 118301. (doi:10.1103/PhysRevLett.106.118301)
32. Dorfmann A, Ogden RW. 2006 Nonlinear electro-elastic deformations. *J. Elast.* **82**, 99–127. (doi:10.1007/s10659-005-9028-y)
33. Suo ZG, Zhao XH, Greene WH. 2008 A nonlinear field theory of deformable dielectrics. *J. Mech. Phys. Solids* **56**, 467–486. (doi:10.1016/j.jmps.2007.05.021)
34. Dorfmann L, Ogden RW. 2017 Nonlinear electro-elasticity: material properties, continuum theory and applications. *Proc. R. Soc. A* **473**, 20170311. (doi:10.1098/rspa.2017.0311)
35. Dorfmann L, Ogden RW. 2019 Instabilities of soft dielectrics. *Phil. Trans. R. Soc. A* **377**, 20180077. (doi:10.1098/rsta.2018.0077)
36. Bertoldi K, Gei M. 2011 Instabilities in multilayered soft dielectrics. *J. Mech. Phys. Solids* **59**, 18–42. (doi:10.1016/j.jmps.2010.10.001)
37. Goshkoderia A, Rudykh S. 2017 Electromechanical macroscopic instabilities in soft dielectric elastomer composites with periodic microstructures. *Eur. J. Mech. A Solids* **65**, 243–256. (doi:10.1016/j.euromechsol.2017.04.008)
38. Bortot E, Shmuel G. 2018 Prismatic bifurcations of soft dielectric tubes. *Int. J. Eng. Sci.* **124**, 104–114. (doi:10.1016/j.ijengsci.2017.11.002)
39. Destrade M, Ní Annaidh A, Coman CD. 2009 Bending instabilities of soft biological tissues. *Int. J. Solids Struct.* **46**, 4322–4330. (doi:10.1016/j.ijsolstr.2009.08.017)
40. Nayfeh AH. 1995 *Wave propagation in layered anisotropic media: with application to composites*, vol. 39. Amsterdam, The Netherlands: Elsevier.

41. Su YP, Wu B, Chen WQ, Lü CF. 2018 Optimizing parameters to achieve giant deformation of an incompressible dielectric elastomeric plate. *Extreme Mech. Lett.* **22**, 60–68. (doi:10.1016/j.eml.2018.05.004)
42. Su YP, Wu B, Chen WQ, Destrade M. 2019 Finite bending and pattern evolution of the associated instability for a dielectric elastomer slab. *Int. J. Solids Struct.* **158**, 191–209. (doi:10.1016/j.ijsolstr.2018.09.008)
43. Melcher JR. 1973 Electrohydrodynamics. In *Theoretical and applied mechanics* (eds E Becker, GK Mikhailov), pp. 240–263. Berlin, Germany: Springer.
44. Fu YB, Dorfmann L, Xie YX. 2018 Localized necking of a dielectric membrane. *Extreme Mech. Lett.* **21**, 44–48. (doi:10.1016/j.eml.2018.03.005)